Model Impacts of Entrainment and Detrainment Rates in Shallow Cumulus Convection

A. P. SIEBESMA AND A. A. M. HOLTSLAG*

Royal Netherlands Meteorological Institute, De Bilt, the Netherlands

(Manuscript received 14 December 1996, in final form 19 January 1996)

ABSTRACT

A mass flux parameterization scheme for shallow cumulus convection is evaluated for a case based on observations and large eddy simulation (LES) results for the Barbados Oceanographic and Meteorological Experiment (BOMEX). The mass flux scheme is embedded in a one-column model with prescribed large-scale forcings. Comparing the findings of the latter with the LES results, it is found that the mass flux scheme is too active. As a result, the scheme is mixing too much heat and moisture between the cloud layer and the inversion layer, giving rise to erroneous moisture and temperature profiles for the trade wind region. This is due to an underestimation of the lateral exchange rates. LES results show that for shallow cumulus cloud ensembles (lateral) entrainment and detrainment rates are typically one order of magnitude larger than values used in most operational parameterization schemes and that the detrainment rate is systematically larger than the entrainment rate. When adopting these enhanced rates, the mass flux scheme produces realistic mass fluxes and cloud excess values for moisture and heat and is therefore capable of maintaining the stationary state as observed during BOMEX.

1. Introduction

Shallow cumulus convection is one of the important mechanisms that needs to be parameterized in atmospheric climate and weather forecast models. The relevance of these clouds for large-scale atmospheric dynamics is most clearly demonstrated in the trade wind areas above the oceans. In these subtropical belts, the surface evaporation from the ocean increases significantly due to the enhanced mixing of heat and moisture of these trade wind cumuli. This moisture is transported downstream by the trade winds into the intertropical convergence zone (ITCZ) where it is finally released as latent heat in deep convective intertropical disturbances. Since this latent heat release in the ITCZ enhances the Hadley circulation, the surface evaporation upstream in the undisturbed trade wind areas can be regarded as a fuel supply for this circulation. It is in this context that the presence of trade wind cumuli intensifies the large-scale circulation. Also, locally it is important to include the effects of vertical mixing of heat and moisture by trade wind cumuli in atmospheric modeling to counteract the drying and warming effects of the large-scale subsidence induced by the Hadley circulation. As a result, a thermodynamic steady state of the cloud and inversion layer in the undisturbed trade wind regions can be maintained.

To gain more insight into the physical mechanism of shallow cumulus convection, Siebesma and Cuijpers (1995, hereafter SC95) have utilized a large eddy simulation (LES) model and succeeded in making a realistic steady-state run based on data from the Barbados Oceanographic and Meteorological Experiment (BOMEX) (Holland and Rasmusson 1973). The output of the LES results has been used in SC95 to test elementary assumptions usually made in mass flux parameterizations. One of the most important results of that study was related to entrainment and detrainment rates that describe the mass exchange between clouds and the environment. The LES results indicated that these rates should be almost one order of magnitude larger than values used in operational shallow convection parameterizations (Tiedtke 1989; Gregory and Rowntree 1990).

The objective of this paper is to compare a typical shallow cumulus parameterization embedded in a representative atmospheric model with the LES results obtained in SC95. For this purpose we use a one-column version of the ECHAM3 climate model (Roeckner et al. 1992). This model has been developed from the European Centre for Medium-Range Weather Forecasts (ECMWF) model, which is a "state of the art" medium-range weather forecast model (Simmons et al.

* Additional affiliations: Institute of Marine and Atmospheric Research, University of Utrecht, the Netherlands, and the National Center for Atmospheric Research, Boulder, Colorado.

Corresponding author address: Dr. Pier Siebesma, KNMI, P.O. Box 201, 3730 AE De Bilt, the Netherlands.
E-mail: siebesma@knmi.nl

1989). In both models cumulus convection is described by a mass flux scheme proposed by Tiedtke (Tiedtke 1989, hereafter T89). We will be mainly concerned with the entrainment and detrainment rates used in the mass flux scheme. The main question we would like to answer in this paper is whether the performance of the scheme actually improves when using the enhanced rates as suggested by the LES results.

The organization of this paper is as follows. The basics of the cumulus scheme and the approximations involved are presented in section 2. The relevant LES results for the BOMEX case as obtained in SC95 are discussed in section 3. In section 4, we present the results of the one-column model. Runs are made and discussed with the standard operational entrainment and detrainment rates and with the enhanced rates as suggested by the LES data. In the appendix, the impact of these revised rates is discussed on the basis of analytical solutions for the mass flux scheme. Finally, in section 5 the results and implications are discussed.

2. Cumulus convection

a. Basics

The prognostic large-scale equations for the liquid water potential temperature θ_l and the total water specific humidity q_t can be written within the quasi-Boussinesq approximation as

$$\frac{\partial \overline{\theta_l}}{\partial t} + \nabla\cdot(\overline{\mathbf{v}}\,\overline{\theta_l}) + \frac{\partial(\rho\overline{w}\overline{\theta_l})}{\rho\partial z} = -\frac{\partial(\rho\overline{w'\theta_l'})}{\rho\partial z} + c_p Q_r$$

$$\frac{\partial \overline{q_t}}{\partial t} + \nabla\cdot(\overline{\mathbf{v}}\,\overline{q_t}) + \frac{\partial(\rho\overline{w}\overline{q_t})}{\rho\partial z} = -\frac{\partial(\rho\overline{w'q_t'})}{\rho\partial z}, \quad (2.1)$$

where ρ is the average density, $\mathbf{v}$ the horizontal velocity, w the vertical velocity, and Q_r the radiative heating rate. Overbars denote a spatial horizontal average over the grid area A of a large-scale model [typically $(50)^2 \sim (200)^2$ km^2], and the primes denote deviations from the horizontal average. Horizontal turbulent transport terms have been neglected in the equations. Since we will consider only nonprecipitating clouds, we have not included sink terms due to rain in the equations. The large-scale advection and subsidence term on the left-hand side of (2.1) are resolved by a large-scale model. The terms on the right-hand side of (2.1) all refer to subgrid processes that need to be parameterized.

In order to decompose (2.1) into separate equations for the active cloudy part and the environmental part, we rewrite the turbulent fluxes of $\chi \in \{\theta_l, q_t\}$ as

$$(\overline{\rho w'\chi'}) = a\rho\overline{w'\chi'}^{c} + (1-a)\rho\overline{w'\chi'}^{e} + a\rho(w_c - \overline{w})(\chi_c - \chi_e)$$

with

$$a\overline{w'\chi'}^{c} \equiv \frac{1}{A}\int\int_{\text{cloudy}} (w - w_c)(\chi - \chi_c)\,dxdy$$

$$(1-a)\overline{w'\chi'}^{e} \equiv \frac{1}{A}\int\int_{\text{env}} (w - w_e)(\chi - \chi_e)\,dxdy, \quad (2.2)$$

where a is the fraction of the active cloudy part and the subscripts c and e label active cloud and passive environmental averages, respectively. The first term (the in-cloud turbulence) describes the correlated fluctuations with respect to the cloud average, and the second term (the environmental turbulence) describes correlated fluctuations with respect to the environmental average. The third term describes the contribution due to organized updrafts in the clouds and compensating subsidence in the environment.

If we now introduce an entrainment rate E and a detrainment rate D, describing the lateral mass exchange between the cloudy and the environmental part, we can write down separate equations for $\chi \in \{\theta_l, q_t\}$ for both parts:

$$\rho\frac{\partial a\chi_c}{\partial t} = -\frac{\partial M_c\chi_c}{\partial z} + E\chi_e - D\chi_c - \frac{\partial \rho a\overline{w'\chi'}^{c}}{\partial z} + \rho\left(\frac{\partial a\chi_c}{\partial t}\right)_{\text{forcing}}$$

$$\rho\frac{\partial (1-a)\chi_e}{\partial t} = +\frac{\partial M_c\chi_e}{\partial z} - E\chi_e + D\chi_c - \frac{\partial \rho(1-a)\overline{w'\chi'}^{e}}{\partial z} + \rho\left[\frac{\partial (1-a)\chi_e}{\partial t}\right]_{\text{forcing}}. \quad (2.3)$$

In (2.3) a mass flux $M_c = a\rho(w_c - \overline{w})$ is introduced, and for simplicity, the advection, the subsidence, and the radiation terms from (2.1) are grouped together in one forcing tendency. A similar decomposition for the mass continuity equation gives

$$\rho\frac{\partial a}{\partial t} = -\frac{\partial M_c}{\partial z} + E - D. \quad (2.4)$$

The set of equations (2.3) and (2.4) can be considered as a starting point for mass flux parameterizations. Next, we briefly review the assumptions that lead to the mass flux parameterization as proposed in T89. Although we focus on one specific cumulus scheme, most of the assumptions are quite generic for other mass flux schemes representing cumulus convection.

b. Parameterizations

A basic assumption in many mass flux schemes is that turbulent transport can be well approximated by major cumulus updrafts and compensating environ-

mental subsidence. This implies that the first two terms of the right-hand side of (2.2) can be neglected. Then a mass flux approximation for the turbulent flux for an arbitrary field χ reads as

$$(\rho\overline{w'\chi'}) \approx M_c(\chi_c - \chi_e). \tag{2.5}$$

From the modeling point of view, the result (2.5) is extremely desirable since it implies that one needs to know only a mass flux M_c and average fields in and outside the clouds to estimate turbulent fluxes. A second approximation is to assume that the cloud cover $a \ll 1$, so that $\chi_e \approx \bar{\chi}$. Finally, it is assumed that the cloud ensemble is in a steady state, so that the tendencies of the cloudy part can be neglected. Applying these three simplifications to the set of equations (2.3) and (2.4) for $\chi \in \{\theta_l, q_t\}$, we arrive at

$$\frac{\partial M_c}{\partial z} = E - D \tag{2.6a}$$

$$\frac{\partial M_c\chi_c}{\partial z} = E\bar{\chi} - D\chi_c \tag{2.6b}$$

$$\rho\frac{\partial\bar{\chi}}{\partial t} = \frac{\partial M_c\bar{\chi}}{\partial z} - E\bar{\chi} + D\chi_c + \rho\left(\frac{\partial\bar{\chi}}{\partial t}\right)_{\text{forcing}}. \tag{2.6c}$$

Equation (2.6c) can be put in an even more transparent form by eliminating the entrainment and detrainment terms using (2.6b):

$$\frac{\partial\bar{\chi}}{\partial t} = -\frac{\partial M_c(\chi_c - \bar{\chi})}{\rho\partial z} + \left(\frac{\partial\bar{\chi}}{\partial t}\right)_{\text{forcing}}. \tag{2.7}$$

This finding simply states that within the mass flux approximation (2.5) the tendency of the conserved variable χ due to convective clouds is equal to the turbulent flux divergence.

To solve the set equations given by (2.6), the entrainment and the detrainment rates are parameterized in terms of the mass flux:

$$E = \epsilon M_c$$
$$D = \delta M_c, \tag{2.8}$$

where fractional entrainment and detrainment rates ϵ and δ are introduced, which in T89 are assumed to be equal and constant,

$$\epsilon = \delta = 3 \times 10^{-4}\ \text{m}^{-1}. \tag{2.9}$$

Knowing the boundary conditions at cloud base and cloud top, the set of equations (2.6) can easily be solved. In T89, the boundary conditions of $\theta_{l,c}$ and $q_{t,c}$ at cloud base are determined by lifting a parcel from the lowest model level near the surface to the first model level where condensation occurs. The height of this level of condensation (LCL) is taken to be the cloud-base height z_b. A key closure assumption is the boundary condition of the mass flux M_c at cloud base. This is determined in T89 by the condition that the total moisture content in the dry boundary layer has to remain constant. Provided that the boundary-layer parameterization scheme has a zero turbulent flux at cloud base, this implies that the turbulent mass flux of q_t at cloud base is equal to the surface evaporation plus the moisture convergence by large-scale advection into the boundary layer:

$$[M_c(q_{t,c} - \bar{q}_t)]_{z_b} = (\overline{w'q_t'})_{\text{surf}} + \int_0^{z_b}\left(\frac{\partial\bar{q}_t}{\partial t}\right)_{\text{adv}} dz. \tag{2.10}$$

The cloud top is defined as the highest level where the cloud field is still buoyant with respect to the environment. Once these boundary conditions are determined, one can simply obtain the cloud fields by vertical integration of (2.6). This integration is stopped at cloud top, where, in addition to the lateral detrainment in (2.8), a massive detrainment is assumed to be present. This ensures that the mass flux diminishes to zero at cloud top.

3. Case description and large eddy simulation results

In a large-eddy simulation model the resolution is such that the largest eddies of the turbulence can be resolved, whereas the smaller eddies are described by the well-known scaling behavior in the inertial subrange. The results of a simulation with a cloud-resolving model such as an LES model is therefore an ideal tool to test parameterization assumptions. Here we use the LES model developed by Cuijpers and Duynkerke (1993).

In SC95 a large eddy simulation has been made on the basis of the undisturbed period of phase 3 during BOMEX (Holland and Rasmusson 1973; Nitta and Esbensen 1974). During this period, nonprecipitating clouds were the only type of cumuli that were observed under steady-state conditions. Initial profiles of the total water specific humidity q_t, the liquid water potential temperature θ_l, and the horizontal velocity components u and v are shown in Figs. 1a,b along with observations. The large-scale-forcing contributions that can not be calculated by the LES model have been prescribed using results of budget studies from BOMEX (Holland and Rasmusson 1973). These contributions include the large-scale subsidence (Fig. 2a), the large-scale horizontal gradient of q_t (Fig. 2c), and the geostrophic wind (Fig. 1b). The large-scale gradients of θ_l and v are taken to zero, and the large-scale gradient of u follows from the subsidence profile using the continuity equation. Since it was a case with a low cloud cover, it was not necessary to use an interactive radiation scheme. Instead, radiative cooling has been prescribed

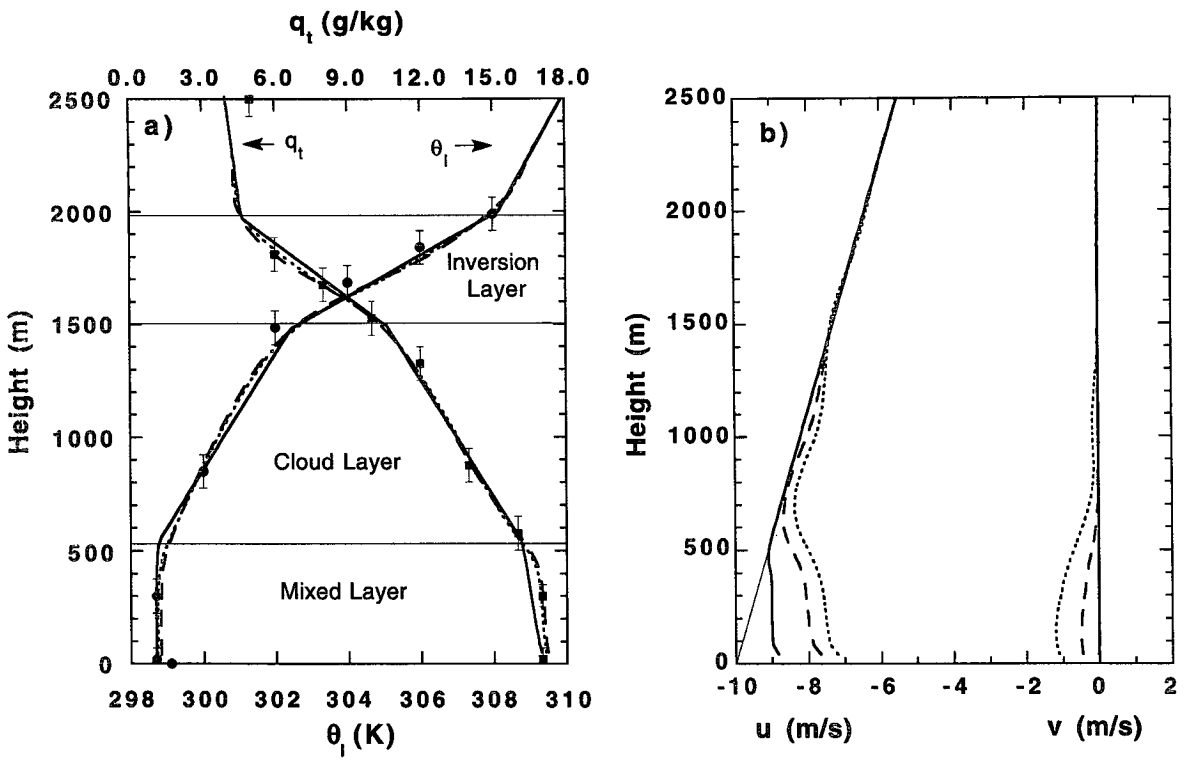

FIG. 1. Horizontally averaged vertical profiles of the LES output for (a) the liquid water potential temperature θ_l and the total water specific humidity q_t and (b) the wind components u and v at time $t = 0$ h (full lines), $t = 3$ h (dashed lines), and $t = 7$ h (dotted lines). The circles and squares are observed values from BOMEX. The thin line in (b) is the prescribed geostrophic wind profile.

as indicated in Fig. 2b. For a more detailed description and motivation of the initial profiles and the forcing terms, we refer to SC95.

Using the large-scale forcing and the initial profiles as described above, an LES run of 7 h has been performed. After about 3 h, the cloud field was well developed and in equilibrium with the large-scale forcing. Figures 1a,b show, besides the initial profiles, the mean profiles of θ_l, q_t, u, and v after 3 and 7 h. From these figures it is clear that the fields of thermodynamical interest, that is, θ_l and q_t, are in an acceptable steady state. We can therefore conclude that the cloud ensemble is in balance with its forcing. An additional advantage of the steady state is that time averaging is allowed to improve the statistics of the cloud ensemble. The output of the LES has been used in SC95 mainly to investigate two important parameterization issues. Let us briefly discuss those results that are relevant for the present study.

The validity of the mass flux approximation (2.5) has been tested in SC95 by calculating both the rhs and the lhs using LES output. For the conserved

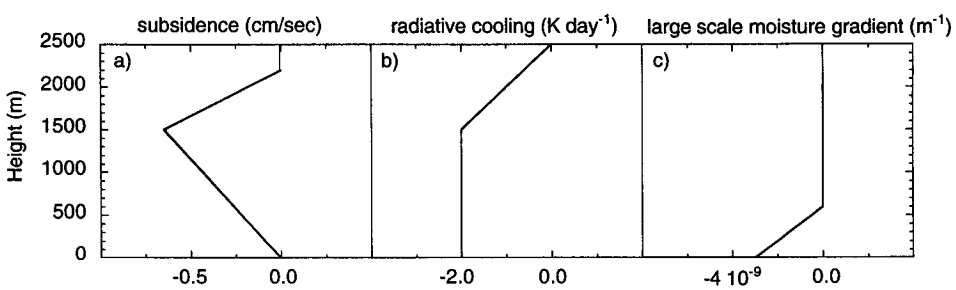

FIG. 2. Profiles of the main components of the prescribed forcings: (a) the large-scale vertical velocity, (b) the radiative cooling, and (c) the large-scale zonal gradient of the specific humidity q_t.

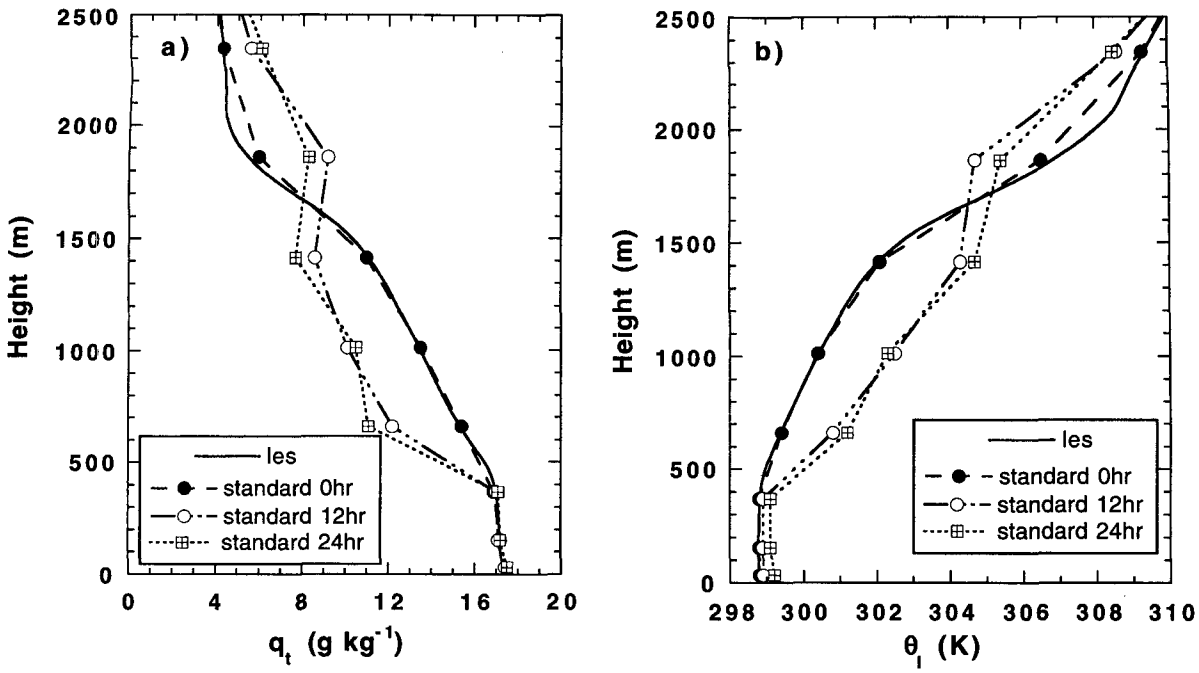

FIG. 3. One-column run results: average profiles of (a) the total water specific humidity q_t, and (b) the liquid water potential temperature θ_l for the standard run after 0, 12, and 24 h. For comparison we also show the steady-state profiles of the LES output.

fields q_t and θ_l, reasonably good results were found: the mass flux approximation [i.e., the rhs of (2.5)] could explain 70% ~ 90% of the total turbulent flux. Only near cloud base were larger deviations found, due to the fact that the environmental turbulence term [see (2.2)] gives a significant contribution. These results indicate that a mass flux scheme is a very appropriate way to parameterize transport due to convective clouds.

Fractional entrainment and detrainment rates for the cloud core have been determined from the LES output in SC95 as residuals from (2.3) and (2.4). The following typical values were obtained:

$$\epsilon \approx 1.5 \sim 2.5 \ (\times 10^{-3}\ \mathrm{m}^{-1})$$
$$\delta \approx 2.5 \sim 3 \ (\times 10^{-3}\ \mathrm{m}^{-1}). \qquad (3.1)$$

The spread in the results of (3.1) is mainly due to variation of the rates with height. Various sensitivity tests have been made by varying the resolution and domain size of the LES model. In all cases however the fractional entrainment and detrainment rates remained within the range indicated by (3.1). Note that these values appear to be one order of magnitude larger than those used in T89 and that $\delta > \epsilon$. In the next section we will investigate the impact of the revised exchange rates (3.1) on the mass flux parameterization for BOMEX.

4. Testing the convection scheme using a one-column model

To test the impact of the entrainment and detrainment rates for the convection scheme in a large-scale model environment, we utilize a 31-level, one-column model that is derived from the ECHAM3 climate model (Roeckner et al. 1992). For the present simulation only the lowest eight levels are active: 34, 155, 370, 661, 1013, 1416, 1863, and 2346 m. A one-column model is merely the parameterization package of the full model. As input, it needs initial profiles and a prescribed forcing such as large-scale advection and subsidence. As a response, it computes the parameterized subgrid processes, such as surface fluxes, vertical turbulent mixing, condensational effects, precipitation, and radiation. To focus on the turbulent mixing processes, we have prescribed the radiative cooling and the surface fluxes. As a result, the only active parameterization schemes are the cumulus convection scheme and the boundary-layer scheme for the turbulent mixing in the subcloud layer. For the latter a local diffusion scheme is used, as proposed by Louis (1979).

We have made runs based on BOMEX for two cases: 1) a standard run with the operational values for ϵ and δ given by (2.9), and 2) a revised run with $\epsilon = 2 \times 10^{-3}\ \mathrm{m}^{-1}$ and $\delta = 2.7 \times 10^{-3}\ \mathrm{m}^{-1}$, as suggested by the LES results (3.1). The one-column model was initialized with profiles produced by the LES model

after 3 h of simulation (see Fig. 1). The prescribed large-scale forcing, radiative cooling, and surface fluxes were the same as in the LES run. Since we are mainly interested in the thermodynamics, we also have prescribed the wind field as given by the LES model.

We have run the one-column model until it reached a steady state and the profiles became time independent. Ideally, the physics of the parameterization scheme has to counteract the large-scale forcing, and the resulting profiles should remain stationary from the very beginning. For the standard run we show in Figs. 3a,b the average profiles of q_t and θ_l after 0, 12, and 24 h. These results show that the convection scheme is overactive. Too much heat and moisture is mixed between the cloud layer and the inversion. As a result, the model is tending to a new equilibrium, reached after 12 h, where the cloud layer is too dry and too warm and the inversion has completely disappeared.

Results for the revised run are displayed in Fig. 4, where the average profiles of q_t and θ_l after 0, 12, and 24 h, are shown. The tendencies of the various processes, averaged over the last 12 h of this run, are displayed in Figs. 5a,b. With the revised values of ϵ and δ, the convection scheme is perfectly balancing the large-scale forcing. Consequently, the profiles are stationary from the very beginning, in agreement with the observations and the LES results.

Since the turbulent flux is (within the mass flux approximation) simply the product of the convective mass flux M_c and the cloud excess value $(\chi_c - \bar{\chi})$ [see (2.5)], it is interesting to compare these profiles for both cases with the LES output. The results are shown in Figs. 6a,b and suggest the following:

1) *The convective mass flux.* The LES output indicates that the mass flux is monotonically decreasing with height. The main reason for this is that most clouds have a cloud top well below the inversion and relatively few clouds actually do reach the inversion at 1500 m. As a result, there is a net outflow from cloud mass into the environment all the way from cloud base to cloud top. Similar results for the mass flux have been found by Esbensen (1978), who used a bulk cloud model for the same BOMEX case. In the standard run however the mass flux is constant with height in the whole cloud layer and is only decreasing in the inversion layer, where there is massive detrainment. This is of course due to the fact that the entrainment and detrainment rates were given the same value in the cloud layer [see (2.9)]. As a result, the mass flux, and hence the turbulent fluxes, are overestimated in the standard run. In the revised run, where the fractional detrainment rate is larger than the fractional entrainment rate, the resulting convective mass flux is still slightly too large but resembles the LES output much better. We refer to the appendix for an analytical demonstration of these results.

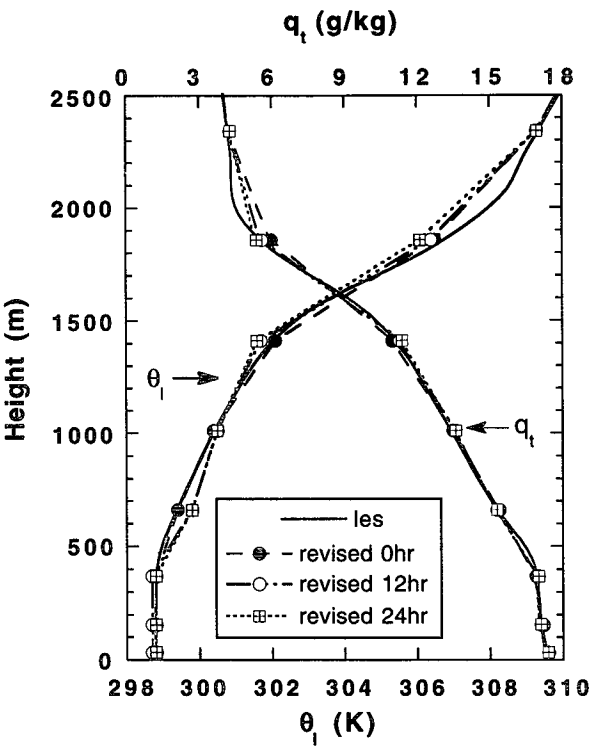

FIG. 4. One-column run results: as in Fig. 3 but with the revised values for the fractional entrainment rate ϵ and fractional detrainment rate δ as suggested by the LES results.

2) *The cloud excess values.* Also here it can be observed that the standard run overestimates these values. As shown in the appendix, the cloud excess is strongly reduced by increasing the fractional entrainment rate ϵ. Indeed, the larger fractional entrainment rate suggested by the LES output gives more realistic results for the cloud excess values in the revised run.

3) *The closure assumption (2.10).* In a steady state, which was the case during the LES run, one finds in general for the turbulent flux at cloud-base height z_b

$$(\overline{w'q_t'})_{z_b} = (\overline{w'q_t'})_{\text{surf}} + \int_0^{z_b} \left(\frac{\partial \bar{q}_t}{\partial t}\right)_{\text{adv}} dz. \quad (4.1)$$

Combining this with the closure assumption (2.10), we find that the mass flux approximation of the turbulent flux is forced to be equal to the total turbulent flux at cloud base:

$$M_c(q_{t,c} - \bar{q}_t) = (\overline{w'q_t'})_{\text{base}}. \quad (4.2)$$

The LES output, however, shows that at cloud base the environmental turbulent flux, that is, the second term on the rhs of (2.2), also gives a significant contribution to the total turbulent flux. In practice this implies that the convective mass flux has to be enhanced in order

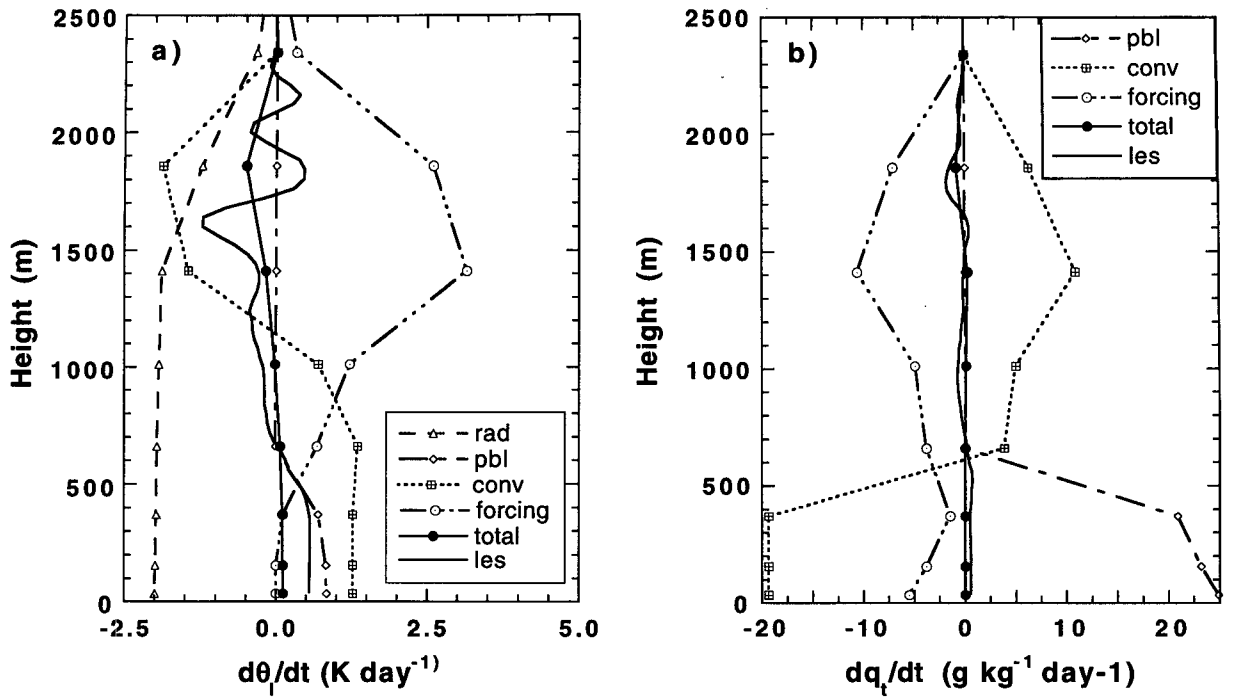

FIG. 5. The tendencies of (a) the liquid water potential temperature θ_l and (b) the total water specific humidity q_t of the various processes in the revised run, averaged over the last 12 h; "rad": radiation scheme, "pbl": boundary layer scheme, "conv": mass flux, "forcing": prescribed large-scale advection and subsidence, "total": total tendency of the one-column model, and "les" total tendency of the LES model.

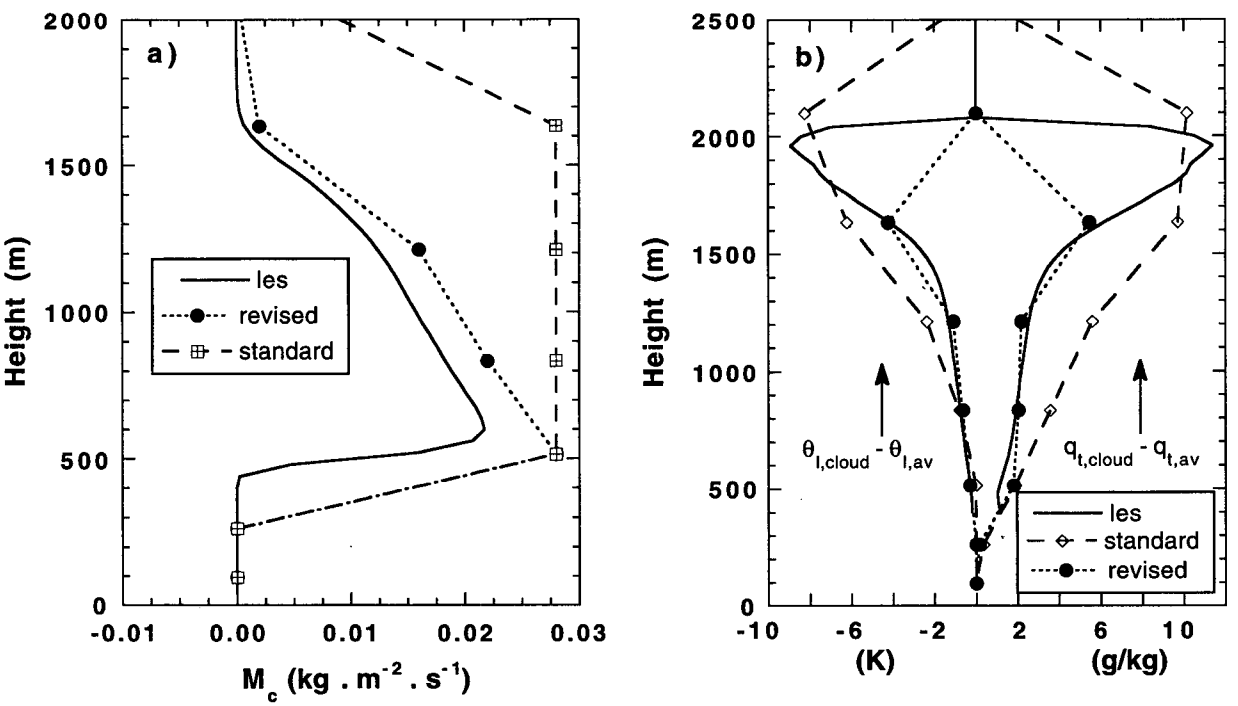

FIG. 6. One-column run results: (a) mass flux profiles for the standard and revised run, and (b) the cloud excess values of q_t and θ_l for the standard and the revised run. For comparison we also show the steady-state mass flux and cloud excess profiles of the LES output.

to obey (4.2). This explains the overestimation for the mass flux at cloud base shown in Fig. 6a for both cases.

5. Discussion

We have presented results of two one-column model runs in comparison with LES results based on BOMEX data. It has been demonstrated that the run using standard values for the fractional entrainment and detrainment rates (ϵ and δ respectively) strongly overestimates the vertical turbulent mixing. The revised run however, where values of ϵ and δ are used as suggested by LES results, produces a realistic steady state in agreement with the observations. These findings promote quite a different picture for the dynamics of shallow cumulus convection. With the standard values of ϵ and δ, the lateral mass exchange is so small that the cloud ensemble acts like a nonleaking funnel (see Fig. 7a). Here moisture and heat are transported almost without loss up to cloud top. The revised run with $\delta > \epsilon$, based on LES results, suggests a rather different physical mechanism (see Fig. 7b) of a funnel that is heavily leaking and is extensively exchanging mass, heat, and moisture all the way from cloud base to cloud top. As a result of the leaking funnel, there is hardly any cloud mass left for massive detrainment at the top, so the inversion does not get excessively moistened and cooled by cloud convection. Most of the mixing is done "on the road" to the inversion within the cloud layer. The physics behind this is that there are a lot of shallow clouds that do not reach the inversion at all and already detrain in the cloud layer below the inversion. Another effect of the stronger entrainment and detrainment is that the zero buoyancy level will be lower. Fortunately, in the present case the bulk cloud remains buoyant until the inversion.

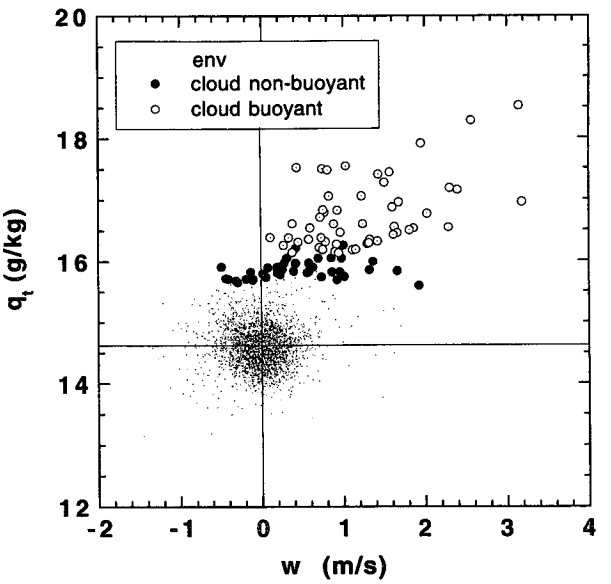

FIG. 8. Scatterplot of the vertical velocity w and the total water specific humidity q_t of a LES simulation at 1200 m. The thin points represent environmental grid points, the open circles buoyant cloudy points, and the solid circles nonbuoyant cloudy points.

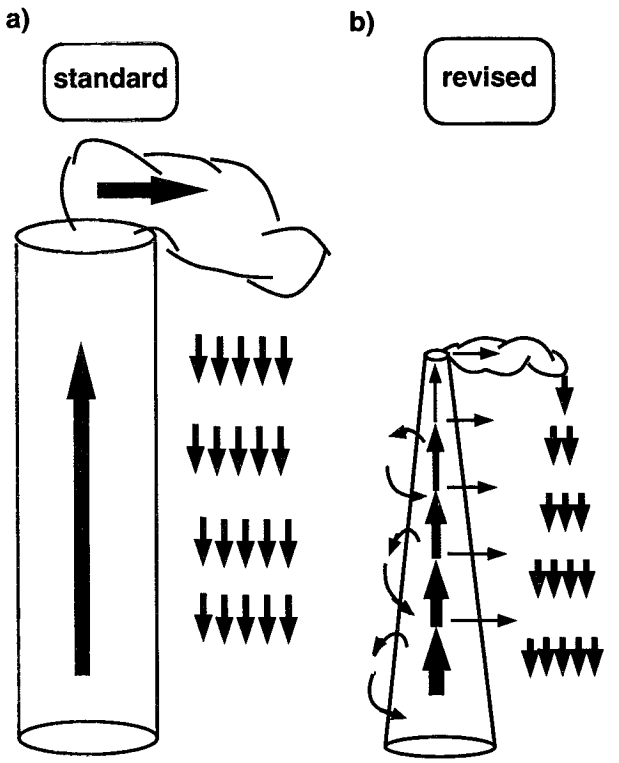

FIG. 7. Schematic picture of the turbulent mixing mechanism of a shallow cloud ensemble. In the case of the standard values of ϵ and δ, the scheme behaves approximately as a nonleaking funnel with massive detrainment at cloud top. When using the enhanced values of ϵ and δ, as suggested by the LES results, there is more intense lateral mixing and a decreasing mass flux with height due to the fact that $\delta > \epsilon$ and hence little massive detrainment at the top.

The success of a mass flux approach can also be demonstrated graphically. In Fig. 8 we show a scatterplot of values for q_t and w for all grid points of the LES model at 1200 m. A distinction has been made between environmental grid points (no liquid water), buoyant cloudy grid points, and nonbuoyant cloudy grid points. It can be seen that most of the upward vertical transport is carried by the buoyant cloudy points. Moreover, the cloudy points are well separated from the environmental points, resulting in a substantial cloud excess value. These two observations are in favor of the mass flux approximation (2.5). It can be further observed that the fluctuations of w and q_t in the environment are almost uncorrelated; that is, the environmental points spread isotropically. Therefore, the environmental turbulence [the second term on the rhs of (2.2)] can be neglected at this height. The cloudy grid points are positively cor-

related and give a contribution to the in-cloud turbulence [the first term on the rhs of (2.2)], which is still small compared to the mass flux term (2.5) (see also SC95).

Concerning the fractional entrainment and detrainment values ϵ and δ given by (3.1) as suggested by the LES results for BOMEX, one may wonder how applicable these values are for shallow convection in general. Recently, we made a LES run of a shallow cumulus convection case during the second Lagrangian of Atlantic Stratocumulus Transition Experiment (ASTEX) (Bretherton and Pincus 1995; Bretherton et al. 1995). The same analysis for the cloud core entrainment and detrainment processes has been applied. As such, we obtained a rather constant value 1.5×10^{-3} m^{-1} for ϵ, while δ is increasing with height from 3×10^{-3} to 7×10^{-3} m^{-1}. These outcomes reconfirm the LES results for BOMEX in the sense that δ is systematically larger than ϵ and that both rates are roughly one order of magnitude larger than the standard values (2.9).

Let us try to explain these higher values. Typically, the parameterization of entrainment is based on plume models, which have been extensively studied in the 1960s. For a steady-state plume with a radius R that is increasing linearly with height and that is not generating buoyancy, it can be shown by using similarity theory that [see Turner (1973) for a review]

$$\epsilon = \frac{2\alpha}{R}. \tag{5.1}$$

Here α is a proportionality constant of order 0.1, a value obtained from laboratory experiments (Squires and Turner 1962). In most parameterizations of both deep and shallow convection, (5.1) is used to describe the lateral entrainment processes (Arakawa and Schubert 1974; Anthes 1977; Tiedtke 1989; Gregory and Rowntree 1990; Donner 1993). In bulk cloud parameterizations, R is taken to be the radius of a typical cloud of the ensemble. For shallow convection this implies a typical value of 500 ~ 700 m leading to fractional entrainment rates of 3 ~ 4 ($\times 10^{-4}$ m^{-1}) (Tiedtke 1989; Gregory and Rowntree 1990).

The findings in this paper indicate that such a value is too low. Several possible reasons for this apparent paradox can be given. First, one may doubt the applicability of (5.1) for a cloud ensemble. This relation has been derived for plumes that are in a steady state and that do not produce buoyancy. Clearly, such conditions do not apply to individual clouds that do produce buoyancy and are never close to a steady state. Moreover, even if (5.1) would be valid for individual clouds, then it is still not appropriate to use an effective ϵ for a whole cloud ensemble using a typical radius R. To estimate ϵ of an ensemble, one has to take a weighted average, where the weight of each subset of clouds with identical radii is determined by the mass flux of that subset (SC95). Indeed, spectral cloud analysis of shallow convective clouds (Nitta 1975) shows a broad distribution of cloud tops (and hence of cloud radii) where the mass flux of small clouds is dominant. This might explain the higher values of ϵ we obtained with the LES model.

For the detrainment process no analog results like (5.1) exist, nor experimental results from the laboratory. A detrainment parameterization like (2.8) is rather ad hoc, and a theory is awaiting.

We do not claim that the values for ϵ and δ used in this study are universal constants. It is quite possible that ϵ and δ vary with the environmental conditions in which shallow convection occurs. More research is needed to resolve this issue. The present study shows however that the mass flux concept is a sound approach for the parameterization of vertical transport by shallow cumulus convection, provided that appropriate values for ϵ and δ are used.

Acknowledgments. We would like to thank Michael Tiedtke and Aad van Ulden for interesting discussions and Erik van Meijgaard for his help in setting up the one-column model. We are also grateful to him, Anton Beljaars, and Willemien van Hoeve for a critical reading of the manuscript. Finally, we would like to thank three anonymous referees for many valuable suggestions and comments.

APPENDIX

Analytical Results

Most of the results from the one-column runs with the mass flux scheme can also be understood in a more analytical way. Especially between cloud base height z_b (here at 500 m) and the inversion height z_t (at 1500 m), it is easy to derive some analytical results. In this layer we do not have to take into account the massive detrainment, which is only expected to be present in the inversion layer. We can therefore substitute the parameterization (2.8) for the exchange rates in the cloud model equations (2.6) and obtain for the mass flux M_c and the cloud field $\chi \in \{\theta_l, q_t\}$

$$\frac{\partial \chi_c}{\partial z} = \epsilon(\bar{\chi} - \chi_c)$$

$$\frac{\partial \ln M_c}{\partial z} = \epsilon - \delta. \tag{A.1}$$

Since the slab-average profiles are almost linear and stationary between 500 and 1500 m, we can substitute a linear profile of $\bar{\chi}$ with a constant lapse rate γ:

$$\bar{\chi}(z) = \bar{\chi}(z_b) + \gamma(z - z_b), \quad z_b \leq z \leq z_t, \tag{A.2}$$

in (A.1) and obtain for the mass flux and the cloud excess value

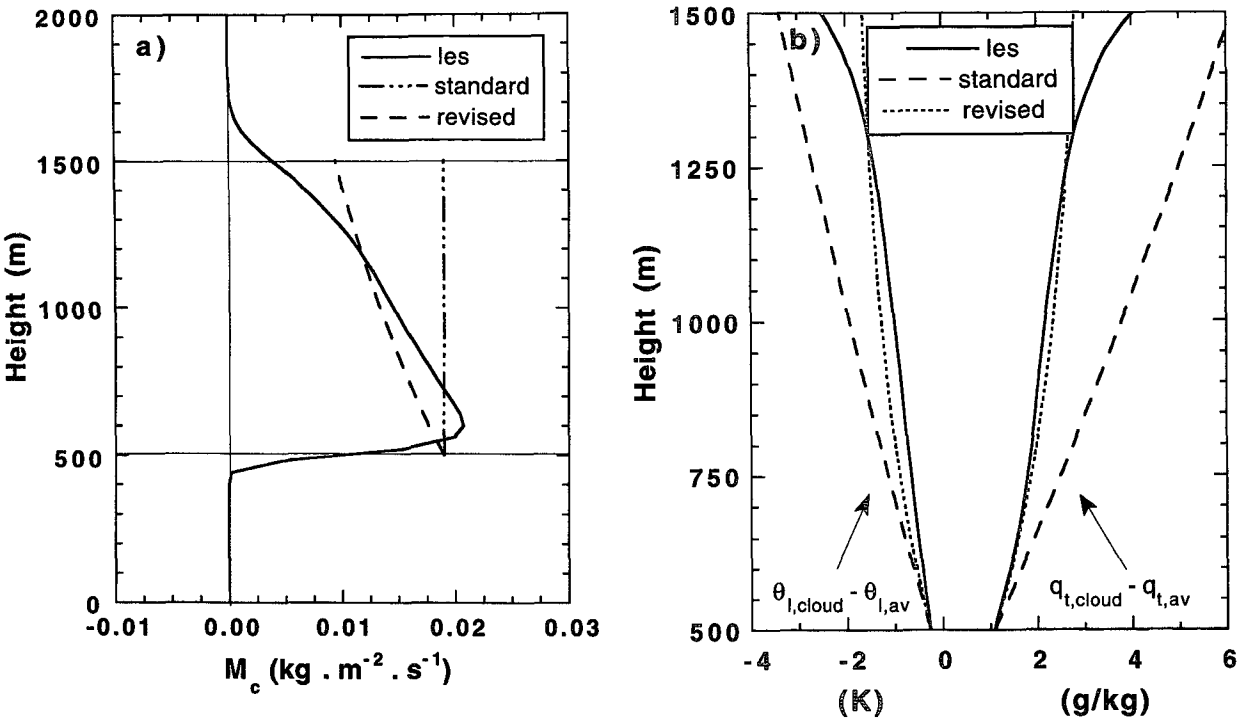

FIG. A1. Results of (a) the mass flux and (b) the cloud excess values of the total water specific humidity and the liquid water potential temperature based on the analytical results of (A.3). For comparison we also show the steady-state mass flux and cloud excess profiles based on the LES output.

$$[\chi_c(z) - \bar{\chi}(z)] = [\chi_c(z_b) - \bar{\chi}(z_b)]e^{-\epsilon z} + \frac{\gamma}{\epsilon}(e^{-\epsilon z'} - 1)$$

$$M_c(z) = M_c(z_b)e^{z'(\epsilon-\delta)}, \qquad \text{(A.3)}$$

with $z' = z - z_b$. Using (2.7), we can easily obtain the tendencies due to cumulus convection $(\partial\bar{\chi}/\partial t)_{cu}$ in terms of ϵ, δ, γ, and the boundary conditions at cloud base,

$$\rho\left(\frac{\partial\bar{\chi}}{\partial t}\right)_{cu} = \gamma M_c(z)\left[1 + \frac{\delta}{\gamma}(\chi_c(z) - \bar{\chi}(z))\right]. \qquad \text{(A.4)}$$

The influence of entrainment and detrainment can be easily observed from these results. In the absence of these lateral mixing processes, that is $\epsilon = \delta = 0$, the equations reduce to

$$M_c(z) = M_c(z_b)$$

$$\chi_c(z) = \chi_c(z_b)$$

$$\rho\left(\frac{\partial\bar{\chi}}{\partial t}\right) = \gamma M_c(z_b). \qquad \text{(A.5)}$$

In that case, we simply have a mass flux and conserved cloud fields that are constant with height and a resulting tendency that is completely due to compensating subsidence. When entrainment and detrainment are switched on, the mass flux will increase or decrease exponentially with height, depending on the sign of $(\epsilon - \delta)$, and the cloud excess value $\chi_c - \bar{\chi}$ will be reduced. Furthermore, the height of the zero buoyancy level, which is used to determine the top of the cloud layer, will be lower if the exchange processes are switched on.

If the parameterization leading to (A.3) is valid, then the correct values of ϵ and δ should give realistic cloud excess values and mass fluxes. We have calculated these profiles using both the standard values of (2.9) and the revised values of ϵ and δ. The mass flux and the fields at cloud base as well as the lapse rates of the average profiles were taken from the LES output. As such, Figs. A1a,b show indeed that the parameterization (A.3) does lead to more realistic mass flux profiles and cloud excess values in the cloud layer, provided that the revised values for ϵ and δ are used.

REFERENCES

Anthes, R. A., 1977: A cumulus parameterization scheme utilizing a one-dimensional cloud model. *Mon. Wea. Rev.*, **105,** 270–286.

Arakawa, A., and W. H. Schubert, 1974: Interaction of a cumulus cloud ensemble with the large-scale environment. Part I: Theoretical formulation and sensitivity tests. *J. Atmos. Sci.*, **31,** 674–701.

Bretherton, C. S., and R. Pincus, 1995: Cloudiness and marine boundary layer dynamics in the ASTEX Lagrangian experiments. Part I: Synoptic setting and vertical structure. *J. Atmos. Sci.*, **52,** 2707–2723.

——, P. Austin, and S. T. Siems, 1995: Cloudiness and marine boundary layer dynamics in the ASTEX Lagrangian experiments. Part II: Cloudiness, drizzle, surface fluxes, and entrainment. *J. Atmos. Sci.*, **52,** 2724–2735.

Cuijpers, J. W. M., and P. G. Duynkerke, 1993: Large eddy simulation of trade-wind cumulus clouds. *J. Atmos. Sci.*, **50,** 3894–3908.

Donner, L. J., 1993: A cumulus parameterization including mass fluxes, vertical momentum dynamics, and mesoscale effects. *J. Atmos. Sci.*, **50,** 889–906.

Esbensen, S., 1978: Bulk thermodynamic effects and properties of small tropical cumuli. *J. Atmos. Sci.*, **35,** 826–837.

Gregory, D., and P. R. Rowntree, 1990: A mass flux scheme with representation of cloud ensemble characteristics and stability-dependent closure. *Mon. Wea. Rev.*, **118,** 1483–1506.

Holland, J. Z., and E. M. Rasmusson, 1973: Measurement of atmospheric mass, energy and momentum budgets over a 500-kilometer square of tropical ocean. *Mon. Wea. Rev.*, **101,** 44–55.

Louis, J.-F., 1979: A parametric model of vertical eddy fluxes in the atmosphere. *Bound.-Layer Meteor.*, **17,** 187–202.

Nitta, T., 1975: Observational determination of cloud mass flux distributions. *J. Atmos. Sci.*, **32,** 73–91.

——, and S. Esbensen, 1974: Heat and moisture budget analyses using BOMEX data. *Mon. Wea. Rev.*, **102,** 17–28.

Roeckner, E., and Coauthors, 1992: Simulation of the present-day climate with the ECHAM model: Impact of model physics and resolution. Max-Planck-Institute Rep. 93, 146 pp. [Available from Deutsches Klimarechenzentrum GmbH, Bundesstrasse 55 D-2000, Hamburg 13, Germany.]

Siebesma, A. P., and J. W. M. Cuijpers, 1995: Evaluation of parametric assumptions for shallow cumulus convection. *J. Atmos. Sci.*, **52,** 650–666.

Simmons, A. J., D. M. Burridge, M. Jarraud, C. Girard, and W. Wergen, 1989: The ECMWF medium-range prediction model, development of the numerical formulations and the impact of increased resolution. *Meteor. Atmos. Phys.*, **40,** 28–60.

Squires, P., and J. S. Turner, 1962: An entraining jet model for cumulonimbus updraughts. *Tellus,* **14,** 422–434.

Tiedtke, M., 1989: A comprehensive mass flux scheme for cumulus parameterization in large-scale models. *Mon. Wea. Rev.*, **117,** 1779–1800.

Turner, J. S., 1973: *Buoyancy Effects in Fluids.* Cambridge University Press, 367 pp.